Unsteady flamelet modeling of CO emissions from a biomass combustor

By E. Knudsen, H. Pitsch, D. J. Cook, K. Kedia AND X. Li

1. Motivation and objective

Biomass fueled combustors are a widely considered (Demirbas 2005) alternative to petroleum and coal fueled combustors. The advantage offered by biomass fuel is that its carbon content has been extracted from the Earth's atmosphere and surface environment. The combustion of these materials is therefore thought to have a minimal impact on atmospheric carbon concentrations. Disadvantages associated with the use of biomass include the material's infrastructure costs (Caputo *et al.* 2005), lower heating value (Demirbas 2005), and complex burning characteristics. For example, biomass materials such as wood pellets are often burned in multi-stage processes (Fletcher *et al.* 2000; Albrecht *et al.* 2008) in which volatile fuel components first gasify and separate from the solid phase material, leaving particles consisting of char and ash. The volatile gases contain significant concentrations of CO and H_2 that can be burned in a secondary process in which additional oxidizer is introduced.

Predictive modeling of biomass combustors requires physical descriptions of processes such as pyrolysis, particle tracking, fluid/particle interaction, and turbulence/chemistry interaction. Although turbulence and chemistry interactions are expected to be important in biomass applications, only limited numbers of multi-scale and large eddy simulation studies of these devices exist. Existing work includes that of Fletcher *et al.* (2000), where a Reynolds Averaged Navier-Stokes (RANS) framework was used in conjunction with a particle tracking method and an eddy break-up chemistry model to study the dynamics of a biomass gasifier. The behavior of the system was well described, but it was found that CO and H_2 concentrations at the combustor outlet were difficult to accurately predict. Albrecht *et al.* (2008) employed a presumed Probability Density Function (PDF) premixed flamelet model in a RANS simulation of a biomass grate furnace. The solid phase was not simulated; instead, experimentally measured values of gas phase species were specified as a boundary condition at the bottom of the furnace. Model predictions were generally similar to those obtained with the use of an Eddy Dissipation Concept (EDC) combustion model, but sensitivities to the fuel composition and the air fluxes were noted. Rogerson *et al.* (2007) employed a non-premixed Conditional Moment Closure combustion model in a simulation of a bagasse fueled furnace. The solid phase was accounted for in their study using Lagrangian particle tracking, but it was observed that accurate prediction of CO near the outlet was difficult to achieve.

The goal of this study is to better understand observed inaccuracies in the prediction of CO emissions from biomass combustors. The inaccuracies that the aforementioned studies have raised will be emphasized by first discussing a RANS simulation of a wood-fired combustor in which combustion is described by an EDC model. This approach has difficulty reproducing experimentally measured CO emissions, and these difficulties will be analyzed using an unsteady flamelet modeling framework. The flamelet framework will then be coupled with a Large Eddy Simulation (LES) flow solver and used to simulate the

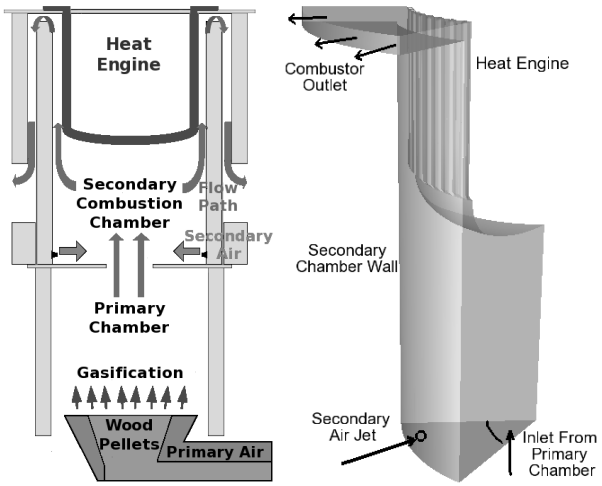

FIGURE 1. Left: schematic of the biomass combustor. Right: schematic of the simulated domain, consisting of a $1/7^{th}$ sector of the cylindrical secondary combustion chamber.

combustor in question. The intention of the study is not to use these simulation results to perform full model validation. Rather, it is to understand the physics that must be captured if the experimentally measured trends are to be reproduced by a model. Results of the flamelet and LES analysis will demonstrate the critical sensitivity that CO has to relationships between turbulent mixing, heat loss, and chemistry.

This introduction forms Section 1 of the study. The biomass combustor that is simulated using RANS and LES is described in Section 2, as are the results of the RANS computations. In Section 3 an unsteady flamelet framework is introduced for the purpose of modeling CO. This flamelet framework is used to study the requirements for accurate CO prediction in Section 4. A LES of the combustor is discussed in Section 5, and Section 6 summarizes the study.

2. Case description

2.1. *Bosch biomass combustor*

Figure 1 shows a schematic of the Robert Bosch Corporation biomass combustor that will be analyzed in this study. Wood pellets and a coflow of air are injected into the device's primary combustion chamber. The pellets gasify, and the resulting gas products are convected through an inlet into a cylindrical secondary combustion chamber with a diameter of $d_{sc} = 0.2$ m.

Symmetrically spaced jets discharge air into this secondary chamber in a direction parallel to the chamber bulkhead. This air provides oxidizer for the combustion of the CO and H_2 species that are found in the primary gas stream. The heat that is released by the oxidation process provides energy to a heat engine that sits at the end of the secondary chamber. The combustion products subsequently convect through an outlet in the secondary chamber's wall and out of the device. The jet Reynolds numbers of the primary and secondary inlets are Re_{fuel}=800 and Re_{air}=4000, respectively.

The secondary combustion chamber will be the focus of all modeling performed in this study. The computational domain that will be used to describe the chamber is shown on

Quantity	Case 1	Case 2
Velocity [m/s]	3.88	3.92
Temp [K]	1370	1377
X_{CO}	0.150	0.165
X_{CO_2}	0.099	0.092
X_{H_2}	0.091	0.101
X_{H_2O}	0.095	0.091
X_{CH_4}	0.010	0.010
X_{N_2}	0.555	0.541

TABLE 1. Experimentally estimated parameters at the primary inlet to the secondary chamber of the wood-fired combustor. X_i denotes the mole fraction of species i.

the right in Figure 1. Because the chamber consists of 7 secondary air jets arranged in an azimuthally symmetric pattern, only a $1/7^{th}$ sector of the chamber is simulated. Standard convective boundary conditions are applied at the combustor outlet. Significant energy is lost through heat transfer to the secondary chamber walls, and these wall temperatures were specified using experimental measurements: 1190 K in the secondary chamber's outer walls, and 800 K along the boundary that defines the heat engine.

Boundary conditions in the secondary combustion chamber's main inlet are estimated using available information: the experimentally measured elemental composition of the wood pellets and the measured temperature of the gas in the primary chamber. These data are used to solve a chemical kinetics equilibrium code and thus estimate the details of minor species concentrations at the inlet. The influence of this equilibrium assumption was analyzed by artificially adjusting the inlet species compositions while holding the mass fractions of each element constant. Simulation results that used the adjusted inlet compositions provided emission predictions that were nearly identical to those that used the assumed equilibrium composition. Sensitivities to the details of the inlet species distributions therefore do not affect the discussion of the model results provided below.

Two cases will be considered in this study, and they will be labeled as case 1 and case 2. The boundary conditions associated with the secondary oxidizer jet are the same in both cases: air at a temperature of 300 K, injected at a velocity of 25 m/s. The details of the primary inlet boundary conditions associated with each case are shown in Table 1. Note that the velocities and compositions of the primary jet streams change only slightly between cases. These marginal inflow changes lead to large changes in the device's CO emissions. This sensitivity to composition changes has been observed over a wide range of operating conditions and is typical of similarly sized biomass combustors. In the RANS simulations shown below, it is assumed that the turbulent fluctuations in the primary inlet have a magnitude of 5% of the bulk inlet velocity. In the LES, the secondary jet is seen to dominate turbulent dynamics near the primary inlet regardless of inflow fluctuations. Both the primary and secondary jets in the LES runs are therefore set as bulk velocity profiles.

The boundary conditions in Table 1 are subject to uncertainties associated with the wood pellet elemental composition, unsteadiness in the feed system, etc. The conditions of cases 1 and 2 are nevertheless very similar, making use of the same wood pellet fuel. In spite of this similarity, the CO concentrations that were experimentally measured at the combustor outlet differ by an order of magnitude. These concentrations are shown in Table 2 along with the measured outlet temperature. The boundary conditions in the

Quantity	Case 1	Case 2
Temp [K]	1080	1090
CO [ppm]	20	130
Z_{outlet}	0.465	0.463

TABLE 2. Secondary combustion chamber outlet conditions.

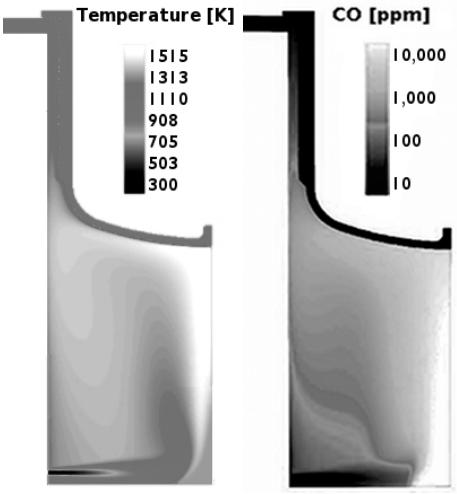

FIGURE 2. Schematic of the case 1 RANS combustion chamber simulation. Left: temperature. Right: CO mole fraction.

primary inlet and the secondary air jet can be used to define a mixture fraction describing the interaction of these two streams (Pitsch & Peters 1998), where the $Z = 0$ condition corresponds to the air jet and the $Z = 1$ condition corresponds to the primary inlet jet. A simple mass balance then provides an estimate of the average mixture fraction value at the outlet. This quantity is also provided in Table 2 and serves as a reference point for the flamelet analysis that will be performed in Section 4.

2.2. *RANS / EDC results*

RANS simulations of the secondary combustion chamber are performed in order to determine whether a standard model can reproduce the measured CO outlet concentrations. The FLUENT code (Fluent 2011) is used for these simulations, and combustion is described by FLUENT's Eddy Dissipation Concept (EDC) model and the GRI 1.2 chemical mechanism (Frenklach *et al.* 1995). A standard $k-\epsilon$ approach is used to account for turbulence. Representative RANS results from case 1 are shown in Figure 2.

The plot on the right side of Figure 2 highlights how CO evolves within the chamber. The large concentrations of CO that enter through the primary inlet evolve under the influence of a variety of physical mechanisms. For example, much of the fluid is deflected by the end of the heat engine, and subsequently is convected in the direction of the outer chamber wall. The fluid might recirculate towards the lower bulkhead and could then linger in the region between the secondary air jet and the heat engine. Eventually, all recirculated fluid will be deflected by the outer chamber wall in the direction of the combustor outlet, and be transported along the thin passage between the heat

Quantity	Case 1	Case 2
CO From RANS [ppm]	52	54

TABLE 3. RANS EDC combustion model CO predictions.

engine and outer wall. Figure 2 suggests that some CO oxidation occurs throughout this representative fluid parcel's traversal of the combustion chamber.

These combustion dynamics highlight the physical processes that affect CO outlet concentrations: turbulent mixing in the jet shear layers and recirculation zone, heat transfer to the walls, and chemical kinetics. In spite of the RANS computation's ability to qualitatively capture these processes, CO concentrations are not quantitatively captured. Table 3 lists the outlet CO concentrations that are predicted by the RANS EDC model. Because of the uncertainty associated with boundary conditions, it is not expected that these values would be in excellent agreement with the experimental measurements. Rather, unlike the experiments, no differences in CO concentrations are observed between case 1 and case 2. An unsteady flamelet modeling framework is introduced to further investigate this lack of sensitivity.

3. Unsteady flamelet model

3.1. *Model formulation*

Unsteady flamelet equations are solved to investigate how CO chemistry evolves in the biomass combustor. These equations have been widely used for modeling (Peters 2000; Pitsch & Ihme 2005; Ihme & See 2010) and can be written in mixture fraction space for the scalar ϕ_i as

$$\frac{\partial \phi_i}{\partial \tau} = \frac{\chi_Z}{2}\frac{\partial^2 \phi_i}{\partial Z^2} + \dot{\omega}_i + \psi_i + \dot{q}_L. \tag{3.1}$$

The dissipation rate of the mixture fraction Z is $\chi_Z = 2\mathcal{D}|\nabla Z|^2$, and $\dot{\omega}_i$ is the chemical source term. The ψ_i term describes transport effects such as molar diffusion correction velocities and differential diffusion effects. The exact form of this term is listed elsewhere (Pitsch & Peters 1998). Unity Lewis numbers are used for all species because the flow field in the combustion chamber is turbulent. The $\dot{q}_L$ term describes heat losses due to, for example, radiation.

3.2. *Heat loss model*

Heat losses influence chemistry in the combustor and must be accounted for in flamelet space. Flamelet models are well suited for describing optically thin radiative heat losses (Marracino & Lentini 1997; Ihme & Pitsch 2008), which are uniquely a function of the species and temperature variables that are explicitly available in mixture fraction space. Flamelet models are less suited for describing wall heat losses, however, because these losses are a function of temperature gradients that are not explicitly available in mixture fraction space.

Modelers have attempted to describe enthalpy losses such as wall heat transfer by imposing enthalpy changes in flamelet space, tabulating the results using an enthalpy variable, and then solving a transported enthalpy equation in physical space to access the various flamelet solutions. For example, van Oijen *et al.* (2001) describe enthalpy changes by varying unburned temperatures in premixed flamelet solutions, while Fiorina

et al. (2003) impose enthalpy changes by stabilizing premixed flamelets artificially rather than in a free stream. The resulting solution sets can be used to describe a variety of heat loss processes.

In Eq. (3.1) all heat losses are considered by means of the loss term $\dot{q}_L$. It will be shown below that the evolution of the CO species is very sensitive to the magnitude of this term. Consequently, radiation cannot be treated as a proxy for wall heat transfer. Instead, the heat loss term $\dot{q}_L$ is treated as a model parameter. In all flamelet calculations, this parameter will be written as a function of temperature according to the empirically chosen formula $\dot{q}_L = \alpha(T - T_0)^2$. A dependence on T^2 rather than radiation's typical dependence on T^4 is chosen because this loss term must describe wall heat transfer as well as radiation. The T^2 dependence is simply an empirical compromise between radiative heat transfer's T^4 dependence and wall heat transfer's T^1 dependence. A baseline temperature of $T_0 =$ 800 K is chosen because this is the coldest wall temperature in the combustor and heat losses are not expected to occur at gas temperatures lower than this. The $\dot{q}_L$ term is set to zero at all flamelet locations where the temperature is less than T_0. The parameter α is varied over four orders of magnitude and ranges from $\alpha = 1 \times 10^{-2}$ $\mathrm{K^{-1}s^{-1}}$ to $\alpha = 1 \times 10^{1}$ $\mathrm{K^{-1}s^{-1}}$. This parameterization of heat loss accounts for all possible combinations of radiation and wall heat transfer in flamelet space.

3.3. *Flamelet solution database*

The unsteady flamelet equations shown in Eq. (3.1) are solved using the FlameMaster program (Pitsch 1998) and the GRI 3.0 chemical mechanism (Smith *et al.* 2000). Flamelet solutions were also generated using the GRI 1.2 mechanism that was employed in the RANS simulation. The CO values in these GRI 1.2 solutions deviated from the GRI 3.0 flamelet solutions by a few ppm at most, indicating that the mechanisms are interchangeable in the context of the current study. The $Z = 0$ boundary condition represents the secondary air jet in the biomass combustor, and is set as air at a temperature of 300 K. The $Z = 1$ boundary condition represents the primary fuel stream, and is set using the data in Table 1. Because these boundary data vary between cases 1 and 2, a unique set of flamelet solutions are generated for each case.

The unsteady flamelet equations are initialized using steady flamelet solutions that are not subject to any heat loss. Steady solutions are used because the primary fuel stream rapidly burns after coming into contact with the secondary air jet. This combustion process occurs more quickly than any of the subsequent mixing, heat loss, or CO oxidation processes. Once initialized, the flamelet profiles are evolved in time according to Eq. (3.1) using a constant dissipation rate profile $\chi_Z(Z)$. As time advances, the heat loss term removes enthalpy from the flamelet and the chemistry adjusts in response. The resulting unsteady flamelet solutions can be parameterized using four variables: 1) the mixture fraction Z that describes the independent flamelet coordinate, 2) the dissipation rate at a reference value of Z, $\chi_{Z,ref}$, 3) the enthalpy variable H that acts as a time-like coordinate, and 4) the heat loss rate $\dot{q}_L$. Mathematically, this relationship is written for the variable ϕ_i as

$$\phi_i = \phi_i(Z, \chi_{ref}, H, \dot{q}_L). \tag{3.2}$$

4. CO predictions

4.1. *Timescale analysis*

Three competing timescales govern the evolution of CO in the secondary combustor: 1) a chemical kinetics timescale represented by $\dot{\omega}_{CO}$, 2) a mixing timescale represented by χ_Z, and 3) a heat loss timescale represented by the α (or $\dot{q}_L$) parameter. Upon first entering the secondary combustion chamber, the primary gas stream mixes with the secondary air jet and burns. During this initial burning phase, combustion is controlled by mixing and the kinetics respond quickly to the local degree of mixing. The steady flamelets that are used for initialization in flamelet space sufficiently describe the interaction of these two timescales. As gas moves farther into the combustion chamber, however, the relative importance of the timescales changes. The mixing timescale increases as gas moves out of the jet shear layers and towards less turbulent flow regions. The kinetics timescale also increases as the initial transients associated with ignition disappear and slower oxidation chemistry becomes important. Eventually these timescales become so large that they overlap in magnitude with the timescale describing heat loss. At locations near the chamber outlet, the flow composition has largely homogenized and the evolution of CO is controlled by a competition between heat loss and chemical kinetics. This competition is active during the last stage of CO evolution before the carrier gas reaches the combustor outlet. The competition between these timescales will now be investigated using the unsteady flamelet results.

4.2. *Unsteady flamelet CO predictions*

Figure 3 compares CO results from two unsteady flamelets that are solved using the same heat loss parameter (α) but different reference dissipation rates ($\chi_{Z,ref}$). As shown in the first plot of this figure, these two flamelets are compared at instances in time at which their maximum temperatures are similar. Although comparisons are made at similar temperatures, the second plot in Figure 3 demonstrates that the high dissipation and low dissipation CO predictions differ by several orders of magnitude. These differences increase as a function of time due to the interaction of the kinetic and mixing timescales. In the higher dissipation rate flamelet (dashed line), mixing occurs relatively fast and transports CO from rich mixture fractions to lean mixture fractions before oxidation kinetics can respond. Conversely, in the lower dissipation rate flamelet (solid line), mixing occurs relatively slowly and CO is oxidized faster than it can be transported in from the rich side of the flamelet. Note that the CO profiles generally have very strong gradients around the mixture fraction value of $Z = 0.46$ that is expected at the combustor outlet.

A second set of flamelet results is plotted in Figure 4. In these two cases the reference dissipation rate ($\chi_{Z,ref}$) is held constant while the heat loss parameter (α) is altered. The flamelets are initialized using the same steady flamelet, and then compared at time instances at which their temperature profiles are similar. The first plot in Figure 4 indicates that the heat loss rate induces only minor structural differences in the temperature profiles of the two flamelets. In the second plot, however, CO is shown to vary by as much as two orders of magnitude when the heat loss rate is changed. At high rates of heat loss, the flamelet temperature decreases much faster than chemical kinetics oxidize CO. After enough heat has been lost, the temperature drops below the cutoff temperature associated with CO oxidation. CO concentrations are consequently relatively unaffected by rapid heat loss. At lower rates of heat loss, significant CO oxidation will occur while the flamelet temperature is decreasing. CO concentrations may then drop to very low levels before the oxidation cutoff temperature is reached. After oxidation ceases, mixing

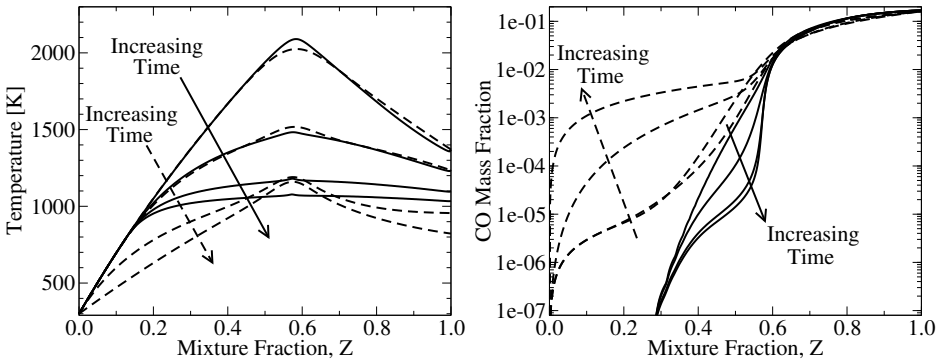

FIGURE 3. CO and temperature from case 1 unsteady flamelets solved using the same heat loss rate $\dot{q}_L$. Solid lines (——): $\chi_{Z,ref} = 1 \times 10^{-3}$ s^{-1}; dashed lines (– – –): $\chi_{Z,ref} = 1 \times 10^{0}$ s^{-1}.

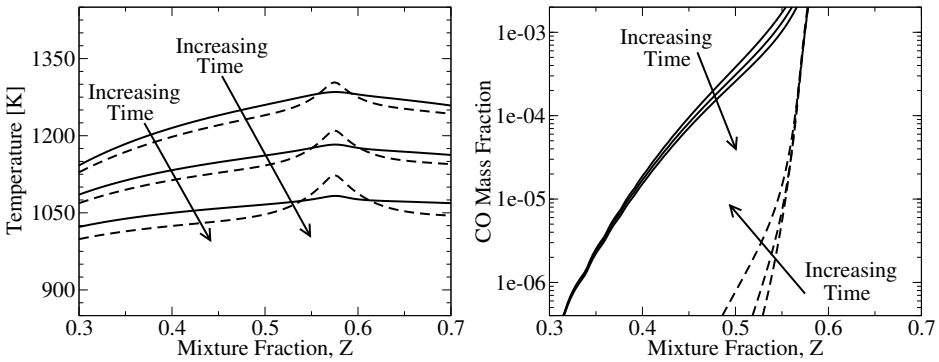

FIGURE 4. CO and temperature from case 1 unsteady flamelets solved using the same $\chi_{Z,ref}$. Solid lines (——): $\alpha = 1 \times 10^{1}$ K^{-1}s^{-1}; dashed lines (– – –): $\alpha = 1 \times 10^{-2}$ K^{-1}s^{-1}.

can begin to transport CO from rich mixture fractions to lean mixture fractions. This transport process leads to the gradual increase in CO concentrations at later times that is depicted by the dashed lines in the second plot of Figure 4.

Figures 3 and 4 demonstrate the extent to which CO is non-linearly sensitive to the interaction of kinetics, mixing, and heat loss timescales. If CO emission sensitivities from the biomass combustor are to be correctly predicted, these interactions must be rigorously and accurately accounted for.

5. Biomass combustor LES

5.1. *LES combustion model*

The unsteady flamelet framework from Eq. (3.2) will now be used to develop an LES combustion model that addresses the outlined modeling needs. Following standard flamelet formulations (Pierce & Moin 2004), the dependence on $\chi_{Z,ref}$ is rewritten in terms of a dependence on a progress variable defined as $C = Y_{H_2O} + Y_{H_2} + Y_{CO_2} + Y_{CO}$. LES filtering is accounted for by presuming that the subfilter distribution of mixture fraction can be described using a beta probability distribution function (PDF) that depends on the filtered mixture fraction, $\widetilde{Z}$, and the subfilter mixture fraction variance, $\widetilde{Z''^2}$. Delta PDFs are presumed for the filtered enthalpy, progress variable, and heat loss rate. Un-

steady flamelet solutions are integrated against beta PDFs, stored in a table, and then accessed as filtered quantities in LES as

$$\widetilde{\phi}_i = \widetilde{\phi}_i(\widetilde{Z}, \widetilde{Z''^2}, \widetilde{C}, \widetilde{H}, \widetilde{q}_L). \tag{5.1}$$

The table is recorded on a five-dimensional mesh of size $110 \times 15 \times 35 \times 35 \times 5$. The 15 points and 5 points that span the variance and heat loss coordinates, respectively, are distributed logarithmically.

Scalar LES transport equations are solved for the $\widetilde{Z}$, $\widetilde{C}$, and $\widetilde{H}$ variables, and an algebraic model is used to determine the subfilter mixture fraction variance (Pierce & Moin 1998). The LES heat loss rate $\widetilde{q}_L$ that appears in the $\widetilde{H}$ equation is calculated in each cell as the sum of radiative heat losses and, at cells adjacent to a boundary, wall heat losses. Radiation is described using an optically thin model that assumes the ambient temperature is equal to the coldest wall temperature of 800 K.

An additional transport equation is solved for the mass fraction of CO. This transport equation is necessary because the final stages of CO oxidation occur over relatively long timescales during which the heat loss and mixing rate around a fluid parcel change. Even in the tabulated unsteady flamelet solutions that account for a time-like variable, a particular history is being assumed for each flamelet. Solving a transport equation for CO minimizes the influence of these assumptions and allows for the decoupling of the history of a flamelet being accessed and the history of a fluid parcel. The chemical source term in the CO equation is modeled using the approach that Ihme & Pitsch (2008) developed for describing source terms in a tranport equation for the NO species. NO forms over timescales that are much longer than those associated with inner flame chemistry, and CO evolves under similar timescale disparities in the biomass combustor. Following Ihme & Pitsch (2008), the CO source term is split into positive and negative components, and the negative component is rescaled using the local transported CO value. The positive and negative source terms are accessed from the table shown in Eq. (5.1).

5.2. *LES flow solver*

LES computations of the biomass combustor are performed on a 2.8 million cell cylindrical mesh that describes the $1/7^{th}$ chamber sector shown in Figure 1. The flow solver is a parallel finite difference code (Desjardins *et al.* 2008) that is advanced in time using a Crank-Nicolson-type second-order implicit scheme. Spatial gradients are calculated using second-order schemes for velocity and third-order schemes for scalars. The code is run in a low-Mach formulation, and a Poisson equation is solved for the pressure variable that enforces mass conservation.

5.3. *LES results*

Contour plots of the mixture fraction, temperature, and CO fields from the LES of case 1 are shown in Figure 5. The intersection of the primary and secondary jets is seen to create a highly turbulent flow field along the centerline of the secondary combustor chamber. Significant CO oxidation occurs as gas moves through this turbulent zone and is convected toward the outer wall. The slower timescales associated with heat loss then become relevant as the CO recirculates along the outer chamber wall and eventually passes by the heat engine on its way to the outlet.

PDFs describing the CO concentrations that pass through the combustor outlet in the LES are shown in Figure 6. The mean values of CO associated with these PDFs are listed in Table 4. Like the EDC combustion model CO predictions, the flamelet predictions have

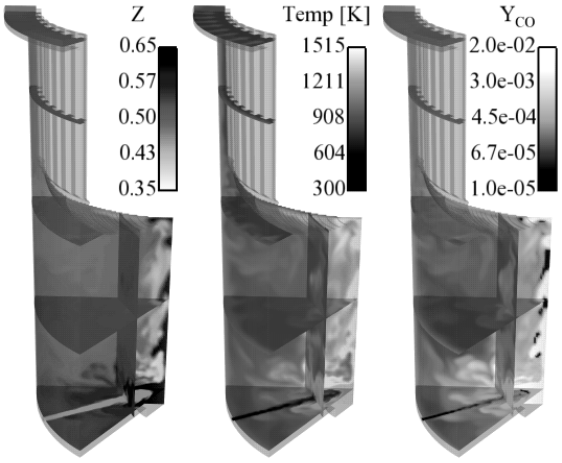

FIGURE 5. Mixture fraction (left), temperature (middle), and CO mass fraction (right) fields in the case 1 LES.

Quantity	Case 1	Case 2
CO From LES [ppm]	290	412

TABLE 4. CO results from the unsteady flamelet LES model.

difficulty reproducing the magnitude of the experimental measurements. Unlike the EDC model, however, the flamelet model is able to reproduce a differential between the case 1 and case 2 emission levels. Note that this differential is reproduced despite the very small change in operating conditions that separates the cases.

This modeling capability is attributed to two advantages that the LES flamelet approach has in comparison to the RANS EDC approach. The first and most important advantage of the flamelet framework is that it more accurately accounts for the small-scale mixing processes that were shown in Figure 3 to have a leading order influence on CO evolution. For example, a small differential in CO can be observed even when single unsteady flamelet solutions representing cases 1 and 2 are compared. These single flamelets therefore describe mixing physics that are uncaptured by the EDC model. When multiple unsteady flamelets are used in a model framework that accounts for heat loss and changing mixing conditions, the differential between the case 1 and case 2 results increases due to the non-linearity of the physics. A second advantage that can be attributed to the LES flamelet approach in particular is its resolution of large turbulent structures. LES resolves mixing processes more accurately than RANS, and thus provides more accurate mixing information to the flamelet framework.

In spite of the advantages of LES, a significant differential between cases 1 and 2 is observed in RANS when the flamelet model is used to describe combustion. Specifically, the use of the unsteady flamelet formulation in the RANS solver described in Section 2 produces CO emissions trends similar to those shown in Table 4. Like the LES implementation, however, the absolute magnitude of the predicted CO emissions exhibit errors.

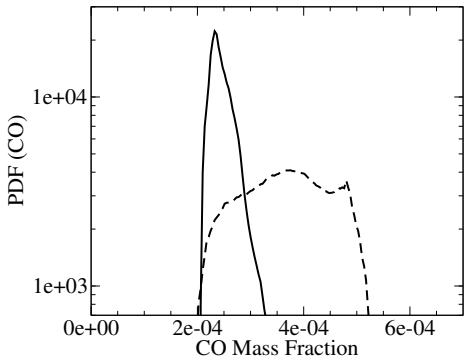

FIGURE 6. Time averaged PDFs from the LES describing CO distributions at the combustor outlet. Solid line (——): case 1; dashed line (– – –): case 2.

6. Summary

This study has investigated the CO emissions of a biomass combustor, and the modeling capabilities that are needed to predict these emissions. A typical RANS approach coupled with an eddy dissipation combustion model was shown to fail to reproduce the sensitivities of experimental CO emissions to a combustor's operating point. In response, an unsteady flamelet framework was introduced and used to investigate the physics that must be described to predict CO. It was demonstrated that mixing, heat loss, and kinetics processes each have a highly non-linear and important influence on CO. This observation suggests that a model must account for boundary conditions, wall heat transfer, and turbulent mixing in a highly accurate manner if it is to be successful. The unsteady flamelet framework was applied in an LES of the biomass combustor, and it enabled the prediction of experimentally observed sensitivities to combustor operation conditions. However, the model was unable to predict the magnitudes of the experimental measurements.

Acknowledgments

Support from the Robert Bosch Corporation through its Research and Technology Center in Palo Alto, California is gratefully acknowledged.

REFERENCES

ALBRECHT, B. A., ZAHIROVIC, S., BASTIAANS, R. J. M., VAN OIJEN, J. A. & DE GOEY, L. P. H. 2008 A premixed flamelet-PDF model for biomass combustion in a grate furnace. *Energy & Fuels* **22** (3), 1570–1580.

CAPUTO, A. C., PALUMBO, M., PELAGAGGE, P. M. & SCACCHIA, F. 2005 Economics of biomass energy utilization in combustion and gasification plants: effects of logistic variables. *Biomass and Bioenergy* **28**, 35–51.

DEMIRBAS, A. 2005 Potential applications of renewable energy sources, biomass combustion problems in boiler power systems and combustion related environmental issues. *Prog. Energy Comb. Sci.* **31** (2), 171–192.

DESJARDINS, O., BLANQUART, G., BALARAC, G. & PITSCH, H. 2008 High order conservative finite difference scheme for variable density low Mach number turbulent flows. *J. Comput. Phys.* **227** (15), 7125–7159.

FIORINA, B., BARON, R., GICQUEL, O., THEVENIN, D., CARPENTIER, S. & DARA-

BIHA, N. 2003 Modelling non-adiabatic partially premixed flames using flame-prolongation of ILDM. *Combust. Theory Mod.* **7**, 449–470.

FLETCHER, D. F., HAYNES, B. S., CHRISTO, F. C. & JOSEPH, S. D. 2000 A CFD based combustion model of an entrained flow biomass gasifier. *Applied Mathematical Modeling* **24**, 165–182.

FLUENT 2011 FLUENT software, Release 12.0. Available from ANSYS Inc., Canonsburg, PA.

FRENKLACH, M., H. WANG, C.-L. Y., GOLDENBERG, M., BOWMAN, C. T., HANSON, R. K., DAVIDSON, D. F., CHANG, E. J., SMITH, G. P., GOLDEN, D. M., GARDINER, W. C. & LISSIANSKI, V. 1995 GRI 1.2. http://www.me.berkeley.edu/gri_mech/.

IHME, M. & PITSCH, H. 2008 Modeling of radiation and nitric oxide formation in turbulent nonpremixed flames using a flamelet/progress variable formulation. *Phys. Fluids* **20** (055110), 1–20.

IHME, M. & SEE, Y. C. 2010 Prediction of autoignition in a lifted methane/air flame using an unsteady flamelet/progress variable model. *Combust. Flame* **157**, 1850–1862.

MARRACINO, B. & LENTINI, D. 1997 Radiation modelling in non-luminous nonpremixed turbulent flames. *Comb. Sci. Tech.* **128**, 23–48.

PETERS, N. 2000 *Turbulent Combustion*. Cambridge, UK: Cambridge Univ. Press.

PIERCE, C. D. & MOIN, P. 1998 A dynamic model for subgrid-scale variance and dissipation rate of a conserved scalar. *Phys. Fluids* **10** (12), 3041–3044.

PIERCE, C. D. & MOIN, P. 2004 Progress-variable approach for Large-Eddy Simulation of non-premixed turbulent combustion. *J. Fluid Mech.* **504**, 73–97.

PITSCH, H. 1998 FlameMaster: A C++ computer program for 0D combustion and 1D laminar flame calculations. Available from http://www.stanford.edu/∼hpitsch/.

PITSCH, H. & IHME, M. 2005 An unsteady/flamelet progress variable method for LES of nonpremixed turbulent combustion. 43^{rd} *AIAA Aerospace Sciences Meeting, Reno, Nevada* pp. 1–14.

PITSCH, H. & PETERS, N. 1998 A consistent flamelet formulation for non-premixed combustion considering differential diffusion effects. *Combust. Flame* **114**, 26–40.

ROGERSON, J. W., KENT, J. H. & BILGER, R. W. 2007 Conditional moment closure in a bagasse-fired boiler. *Proc. Comb. Inst.* **31**, 2805–2811.

SMITH, G. P., GOLDEN, D. M., FRENKLACH, M., MORIARTY, N. W., EITENEER, B., GOLDENBERG, M., BOWMAN, C. T., HANSON, R. K., SONG, S., GARDINER JR., W. C., LISSIANSKI, V. V. & QIN, Z. 2000 GRI 3.0. http://www.me.berkeley.edu/gri_mech/.

VAN OIJEN, J. A., LAMMERS, F. A. & DE GOEY, L. P. H. 2001 Modeling of complex premixed burner systems by using flamelet-generated manifolds. *Combust. Flame* **127** (3), 2124–2134.